Tianjin Daxue Xuebao (Ziran Kexue yu Gongcheng Jishu Ban)/
Journal of Tianjin University Science and Technology
ISSN (Online):0493-2137
E-Publication: Online Open Access
Vol: 59 Issue: 08:2026
DOI: 10.5281/zenodo.22122654

EFFECT OF CURCUMIN-PIPERINE COMBINATION ON TWO IMMUNE CHECKPOINT REGULATORS IN DMBA-INDUCED ORAL SQUAMOUS CELL CARCINOMA

HEND ABDALLA ALSHABRAWY*

Assistant Lecturer, Oral and Maxillofacial Pathology Department, Faculty of Dentistry, Suez Canal University, Kilo 6 Ring Root, Ismailia, Egypt.
*Corresponding Author Email: hend_abdalla@dent.suez.edu.eg;
ORCID: https://orcid.org/0000-0002-6368-1304

MAGDA MOHAMED HASSAN

Professor, Oral and Maxillofacial Pathology Department, Faculty of Dentistry, Suez Canal University, Kilo 6 Ring Root, Ismailia, Egypt. Email: magdahassan1710@gmail.com;
ORCID: https://orcid.org/0000-0003-2235-6035

MERHAN NABIH ELMANSY

Associate Professor, Oral Pathology and Maxillofacial Department, Faculty of Dentistry, Suez Canal University, Kilo 6 Ring Root, Ismailia, Egypt. Email: merhan_elmansy@dent.suez.edu.eg;
ORCID: https://orcid.org/0000-0002-3364-4158

Abstract

Introduction: Oral squamous cell carcinoma (OSCC) remains a leading global malignancy with low survival expectancy due to its evasion from the immune response. Immune checkpoint molecules such as programmed death ligand-1 (PDL-1) and cytotoxic T-lymphocyte antigen-4 (CTLA-4) contribute to tumor immune evasion. Curcumin (Cr), combined with the bioenhancer piperine (Pip), exhibits antiproliferative and anti-inflammatory activities, yet its influence on immune checkpoint expression within a carcinogen-induced tumor microenvironment remains poorly characterized. **Aim:** This study evaluated the short-term effects of an intraperitoneal Cr-Pip combination on tumor progression, systemic cytokine balance, histopathological architecture, and PDL-1/CTLA-4 expression in a DMBA-induced hamster OSCC model. **Methodology:** Twenty male Syrian hamsters were divided into a negative control group (A), a DMBA-induced OSCC positive control group (B), and a DMBA-induced OSCC group receiving one week of intraperitoneal Cr (80 mg/kg) and Pip (1 mg/kg) (C). Tumor size, serum IL-10 and TNF-α, histopathological features, and immunohistochemical PDL-1/CTLA-4 expression were assessed and statistically compared. **Conclusion:** Cr-Pip treatment significantly reduced tumor burden and produced a more cohesive, less invasive histological pattern, accompanied by decreased IL-10, elevated TNF-α, and a significant increase in PDL-1 and CTLA-4 expression. These findings indicate that Cr-Pip modulates both tumor invasive behavior and the immune checkpoints, reflecting a shift toward local immune activation as well as evidence of partial tumor regression.

Keywords: Cytotoxic T-lymphocyte Antigen-4, Curcumin, DMPA Oral Carcinogenesis, Piperine, Programmed Death Ligand-1.

1. INTRODUCTION

Oral squamous cell carcinoma (OSCC) accounts for the large majority of malignant neoplasms affecting the oral cavity. It remains among the most common cancers worldwide, with particularly high incidence in regions where tobacco and areca nut use are prevalent [1]. The persistent clinical challenges in the treatment of OSCC have driven

Tianjin Daxue Xuebao (Ziran Kexue yu Gongcheng Jishu Ban)/
Journal of Tianjin University Science and Technology
ISSN (Online):0493-2137
E-Publication: Online Open Access
Vol: 59 Issue: 08:2026
DOI: 10.5281/zenodo.22122654

sustained interest in understanding the molecular and immunological mechanisms that govern OSCC initiation, progression, and immune evasion, as well as in identifying adjunctive or chemopreventive agents capable of modifying these processes [2] [3].

The hamster buccal pouch (HBP) model, induced by repeated topical application of 7,12-dimethylbenz[a]anthracene (DMBA), remains one of the most extensively validated and histologically faithful animal models of OSCC [4]. It recapitulates the sequential stages of human oral carcinogenesis, from hyperplasia to dysplasia, then invasive squamous cell carcinoma [5]. A growing body of evidence indicates that OSCC progression is shaped not only by the intrinsic proliferative and invasive capacity of tumor cells but also by the tumor's ability to evade immune surveillance [6]. Central to this process are inhibitory immune checkpoint pathways, most notably programmed death ligand-1 (PDL-1) and cytotoxic T-lymphocyte antigen-4 (CTLA-4) [7]. PDL-1, expressed on tumor cells and infiltrating immune cells, engages PD-1 on activated T lymphocytes to suppress cytotoxic T-cell function, while CTLA-4 attenuates T-cell activation at an earlier stage by competing with CD28 for co-stimulatory ligand binding on antigen-presenting cells [8] [9]. Importantly, expression of these checkpoint molecules is not static: it is frequently induced or amplified in response to local immune activation, particularly through interferon-γ signaling released by infiltrating cytotoxic T cells, a phenomenon commonly described as adaptive immune resistance [10].

Natural polyphenolic compounds have attracted considerable attention as potential chemopreventive and adjunctive anticancer agents in OSCC and other epithelial malignancies [11]. Curcumin (Cr), the principal bioactive curcuminoid derived from *Curcuma longa*, has demonstrated antiproliferative, anti-inflammatory, and pro-apoptotic activity in multiple preclinical cancer models, acting through modulation of NF-κB signaling, cyclooxygenase-2 expression, and various pro-inflammatory cytokine pathways [12] [13]. Also, Cr is an effective therapeutic agent mediated through the mitochondrial pathway, which involves upregulation of the Bax/Bcl-2 ratio, cytochrome c release, and activation of caspase-3 [14]. However, the clinical and experimental utility of Cr has historically been constrained by its poor systemic bioavailability, rapid metabolism, and limited absorption following oral administration [15]. Piperine (Pip), an alkaloid derived from *Piper nigrum*, has been shown to substantially enhance the bioavailability of co-administered compounds, including Cr, by inhibiting hepatic and intestinal glucuronidation and modulating drug efflux transporters [16]. Despite this accumulating evidence for the anti-inflammatory and antiproliferative properties of Cr-Pip combinations, relatively little is known about how this combination influences immune checkpoints' expression within the tumor microenvironment in a carcinogen-induced model of OSCC. Furthermore, the short-term systemic effects of a one-week Cr-Pip treatment regimen, administered after OSCC induction, on gross tumor morphology, serum cytokine profile, and histopathological invasive behavior have not been well characterized in this model. The present study evaluated the effects of a short-term (one-week), intraperitoneally administered Cr-Pip combination on tumor progression, systemic inflammatory cytokine profile (IL-10 and TNF-α), histopathological tumor architecture, and immune checkpoint expression (PDL-1 and CTLA-4) in a DMBA-induced hamster model of OSCC. We

Tianjin Daxue Xuebao (Ziran Kexue yu Gongcheng Jishu Ban)/
Journal of Tianjin University Science and Technology
ISSN (Online):0493-2137
E-Publication: Online Open Access
Vol: 59 Issue: 08:2026
DOI: 10.5281/zenodo.22122654

hypothesized that Cr-Pip treatment would reduce tumor burden and modify the local invasive and inflammatory characteristics of the tumor, and that these changes would be accompanied by measurable alterations in immune checkpoint marker expression within the tumor microenvironment, reflecting an underlying shift in local immune activity.

2. MATERIALS AND METHODS

2.1 Ethical approval

The experimental protocol was approved by the Ethical Committee and Faculty Council of the Faculty of Dentistry, Suez Canal University (Approval No. 709/2023). All procedures were conducted in the animal house at Faculty of Dentistry, Suez Canal University.

2.2 Sample size

Sample size estimation was performed using G*Power software (version 3.1.9.7) before initiation of the experiment. Assuming a two-tailed independent-samples *t*-test, a significance level (α) of 0.05, a statistical power of 80%, an allocation ratio of 2:1 (treatment: control), and a large anticipated effect size (Cohen's *d* = 1.5), the minimum required sample size was approximately 20 animals. Based on this calculation and considering ethical principles for animal use, 20 hamsters were included in the study, with 5 animals assigned to each control group and 10 animals allocated to the treatment group.

2.3 Chemicals

One gram of 7, 12-Dimethylbenz[a]anthracene (DMBA; Chongqing Biospes, Cat. No. BCS1807-1) was dissolved in 200 mL of heavy mineral oil (Sigma-Aldrich, USA; Cat. No. 330760) and used as the carcinogen for tumor induction. Cr (Glentham Life Sciences, Cat. No. 458-37-7) and Pip (Sigma-Aldrich, USA; Cat. No. 94-62-2) were used as the treatment compounds. Serum concentrations of IL-10 and TNF-α were measured using Quantikine™ ELISA kits (R&D Systems, USA; Cat. No. D1000B and Cat. No. DTA00D, respectively), according to the manufacturer's instructions. Immunohistochemical evaluation of immune checkpoint markers was performed using a monoclonal anti-PDL-1 antibody (DAKO, Denmark; Cat. No. SK006) and a polyclonal anti-CTLA-4 antibody (ELK Biotechnology; Cat. No. ES8684), with detection performed using the EnVision FLEX+ system (DAKO; Cat. No. K8002).

2.4 Experimental Design and Treatment Protocol

A total of 20 male Syrian golden hamsters (*Mesocricetus auratus*), aged 8–10 weeks and weighing 90–120 g, were used in this study. Animals were housed under standard laboratory conditions with free access to a standard pellet diet and water, and were acclimatized for two weeks prior to start of the experiment. OSCC was induced by painting the left HBP with DMBA using a No. 4 camel-hair brush three times per week for 12 weeks. Animals were randomly assigned to three experimental groups. Group A (n = 5) served as the negative control and did not receive DMBA application. Group B (n = 5) served as the positive control and received DMBA painting. Both Group A and Group B

Tianjin Daxue Xuebao (Ziran Kexue yu Gongcheng Jishu Ban)/
Journal of Tianjin University Science and Technology
ISSN (Online):0493-2137
E-Publication: Online Open Access
Vol: 59 Issue: 08:2026
DOI: 10.5281/zenodo.22122654

animals were euthanized at the end of 12 weeks. Group C (n = 10) underwent the same DMBA induction protocol and subsequently received daily intraperitoneal injections of combined Cr (80 mg/kg) and Pip (1 mg/kg) for one week. Treated animals were euthanized on the second day of the last injection. Euthanasia in all groups was performed via intraperitoneal injection of thiopental sodium (100 mg/kg).

2.5 Clinical evaluation

At the end of each experimental period, animals' body weight was recorded immediately before euthanasia. The HBPs were then examined grossly to assess tumor development and size. High-resolution photographs were taken under standardized conditions and analyzed using FIJI ImageJ software to quantify tumor surface area. Each image was calibrated against a reference scale, and tumor margins were manually delineated to calculate the surface area in mm^2. In animals presenting with multiple tumors, the total cumulative tumor surface area was recorded. All measurements were performed in triplicate under consistent conditions, and the mean of the three readings was used for subsequent statistical analysis.

2.6 Enzyme-linked immunosorbent assay (ELISA)

At the end of each treatment period, before euthanasia, blood samples were collected from anesthetized animals via retro-orbital puncture before euthanasia. Samples intended for ELISA analysis were collected in plain tubes and subsequently centrifuged at 3000 rpm for 10 minutes to separate the serum. The separated serum was collected and stored at −20°C until further ELISA analysis for evaluation of IL-10 and TNF-α.

2.7 Histopathological evaluation

Following euthanasia, all HBP tissue specimens from all groups were fixed in 10% neutral-buffered formalin, processed routinely, and embedded in paraffin. Serial sections of 5-μm thickness were cut and stained with hematoxylin and eosin (H&E) for histopathological evaluation. In stained tumor-bearing specimens, histological features including degree of differentiation, keratin pearl formation, pattern of tumor cell invasion (cohesive versus infiltrative), and extent of stromal infiltration were evaluated. Histopathological assessment was performed independently by two blinded oral pathologists to ensure diagnostic accuracy and minimize observer bias.

2.8 Immunohistochemical evaluation

For immunohistochemical evaluation, 5-μm-thick paraffin sections were mounted on positively charged slides and stained with monoclonal anti-PDL-1 and polyclonal anti-CTLA-4 antibodies, following standard immunohistochemical protocols. Briefly, sections were deparaffinized, rehydrated, and subjected to antigen retrieval, followed by blocking of endogenous peroxidase activity. Sections were then incubated with the respective primary antibodies, followed by incubation with horseradish peroxidase-conjugated secondary antibodies. Immunoreactivity was visualized using diaminobenzidine (DAB) chromogen, and sections were counterstained with hematoxylin. Stained slides were examined microscopically, and representative images were captured using a high-

Tianjin Daxue Xuebao (Ziran Kexue yu Gongcheng Jishu Ban)/
Journal of Tianjin University Science and Technology
ISSN (Online):0493-2137
E-Publication: Online Open Access
Vol: 59 Issue: 08:2026
DOI: 10.5281/zenodo.22122654

resolution digital camera system. To ensure assessment reliability and minimize observer bias, immunohistochemical expression was independently evaluated by two blinded oral pathologists. Quantitative image analysis was performed using FIJI ImageJ software. PDL-1 expression was assessed using both the tumor proportion score (TPS) and the immune cell score (ICS) [17]. CTLA-4 expression was evaluated using the immune cell score (ICS), representing the percentage of positive immune cells within the intratumoral stroma [18].

2.9 Statistical analysis

Descriptive statistics were calculated using Microsoft Excel 365, while statistical analyses were performed with Jamovi software (version 2.7.34). The normality of data distribution was evaluated using the Shapiro–Wilk test. Data are presented as mean ± standard deviation (SD). Comparisons between groups were performed using the Mann–Whitney U test. Statistical significance was defined as $p < 0.05$, with $p < 0.01$ and $p < 0.001$ indicating highly significant and extremely significant differences, respectively.

3. RESULTS

3.1 Clinical observations

Body weight was significantly reduced in tumor-bearing animals compared with the negative control group A. The difference between group A and group C was extremely significant ($p < 0.001$), and a significant difference was also observed between group B and group C ($p < 0.05$) **(Tab.1) (Fig. 1A)**. Gross morphological examination of the HBP displayed normal, tumor-free mucosal architecture in group A, whereas group B developed a large, exophytic, and ulcerated tumor masses characteristic of induced OSCC. In contrast, group C exhibited a visibly smaller tumor mass compared with group B **(Fig. 1B)**. Consistent with the gross findings, tumor size was significantly reduced in the Cr-Pip-treated group ($p < 0.05$) compared to group B **(Tab.1) (Fig 1C)**.

3.2 ELISA results

Serum cytokine analysis revealed distinct inflammatory profiles across groups (Figure 1D). Both IL-10 and TNF-α levels were significantly elevated in group B compared to group A ($p < 0.001$). Following Cr-Pip treatment, group C showed a significant reduction in IL-10 levels compared to group B ($p < 0.001$), while TNF-α levels were significantly elevated relative to group B ($p < 0.01$) **(Tab.1) (Fig 1D)**.

3.3 Histopathological analysis

Histological examination of H&E-stained HBP sections was performed to assess the effect of Cr-Pip treatment on tumor architecture and invasive behavior. Group A (negative control) displayed normal HBP histoarchitecture, characterized by 2–4 layers of well-organized, keratinized stratified squamous epithelium overlying non-inflamed connective tissue and a mature underlying striated muscle layer, with no evidence of dysplastic changes **(Fig. 2A)**.

Tianjin Daxue Xuebao (Ziran Kexue yu Gongcheng Jishu Ban)/
Journal of Tianjin University Science and Technology
ISSN (Online):0493-2137
E-Publication: Online Open Access
Vol: 59 Issue: 08:2026
DOI: 10.5281/zenodo.22122654

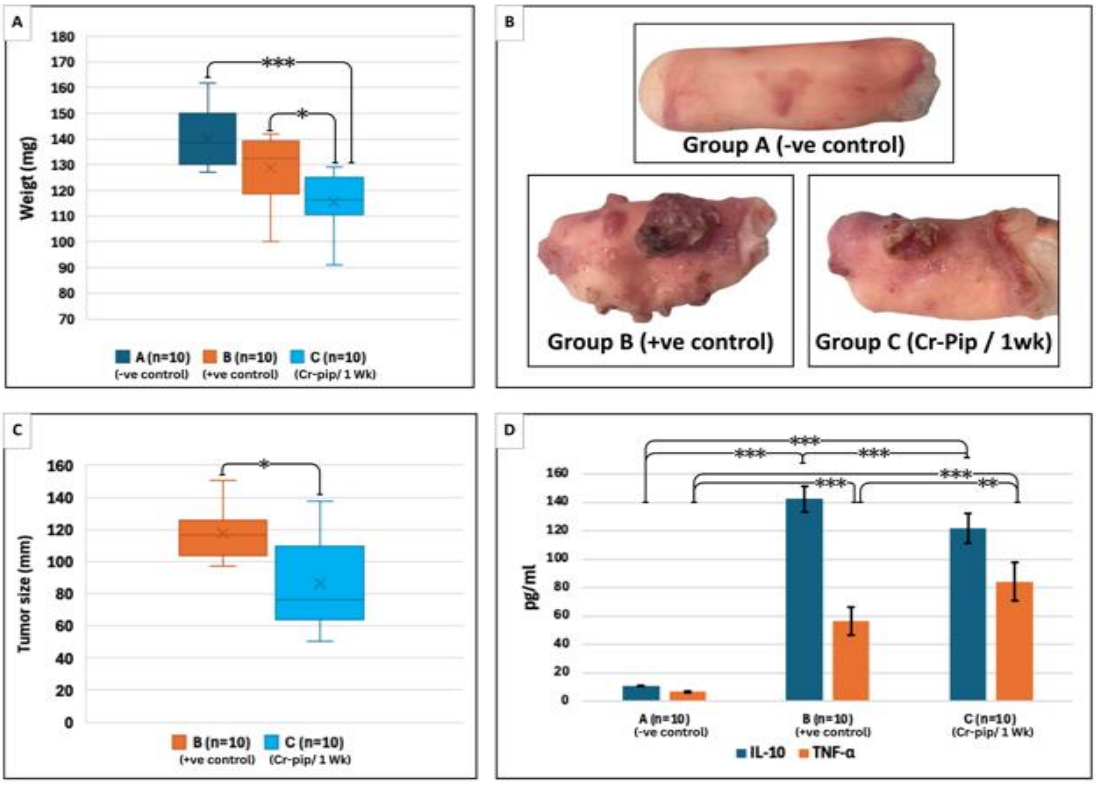

Figure 1: Effects of Cr-Pip treatment on animal weight, tumor progression, and inflammatory cytokine profile in a hamster model. (A) Body weight distribution across experimental groups. Data are presented as box-and-whisker plots. (B) Representative gross morphology of HBP from each group, illustrating tumor formation in Group B and reduced tumor burden following Cr-Pip treatment in Group C, compared with the tumor-free appearance in Group A. (C) Tumor size (mm) comparison between different positive control and treated groups, shown as box-and-whisker plots. (D) Serum concentrations of cytokines IL-10 and TNF-α across the three experimental groups, measured by ELISA. Bars represent mean ± SD. Statistical significance was determined by Mann-Whitney U test (*p < 0.05, **p < 0.01, ***p < 0.001)

Table 1: Statistical analysis of different parameters between the control and treated groups performed using the Mann-Whitney U test. Data are presented as mean ± S.D

Parameter	Groups		Significance
Weight	A* (140.3 ± 10.66)	B* (128.9 ± 12.75)	0.149
	A (140.3 ± 10.66)	C* (115.6 ± 10.70)	<.001***
	B (128.9 ± 12.75)	C (115.6 ± 10.70)	0.021*
Tumor size	B (117.65 ± 18.09)	C (86.19 ± 26.92)	0.025*
IL-10	A (10.02 ± 1.89)	B (142.32 ± 8.41)	<.001***
	A (10.02 ± 1.89)	C (121.72 ± 10.50)	<.001***
	B (142.32 ± 8.41)	C (121.72 ± 10.50)	<.001***
TNF-α	A (7.08 ± 0.81)	B (56.6 ± 9.39)	<.001***

Tianjin Daxue Xuebao (Ziran Kexue yu Gongcheng Jishu Ban)/
Journal of Tianjin University Science and Technology
ISSN (Online):0493-2137
E-Publication: Online Open Access
Vol: 59 Issue: 08:2026
DOI: 10.5281/zenodo.22122654

	A (7.08 ± 0.81)	C (84.22 ± 13.60)	<.001***
	B (56.6 ± 9.39)	C (84.22 ± 13.60)	0.002**
PDL-1 (TPS%)	B (5.62 ± 0.99)	C (8.58 ± 1.26)	0.008**
PDL-1 (CPS%)	B (10.84 ± 1.17)	C (12.98 ± 1.05)	0.008**
CTLA-4	B (1.26 ± 0.06)	C (1.72 ± 0.30)	0.032*
***P-value is considered sigificant at < 0.05**			
****P- value is considered highly signifcant at < 0.01**			
*****P-value is considered extremely significant at < 0.001**			
∗ A (-ve control group), B (+ve control group), C (Cr-Pip/1Wk)			

In contrast, group B (positive control) exhibited features of exophytic SCC, including a deeply invasive, moderately differentiated exophytic tumor mass. Sections from this group showed aggressive infiltration of tumor cells into the underlying connective tissue **(Fig. 2B)**. Following one week of Cr-Pip treatment, group C showed histological features of a moderately differentiated tumor with persistent keratin pearl formation. However, in contrast to Group B, tumor islands in Group C appeared more cohesive, and the invasive front demonstrated a less aggressive growth pattern, with reduced infiltration into the connective tissue stroma **(Fig. 2C)**.

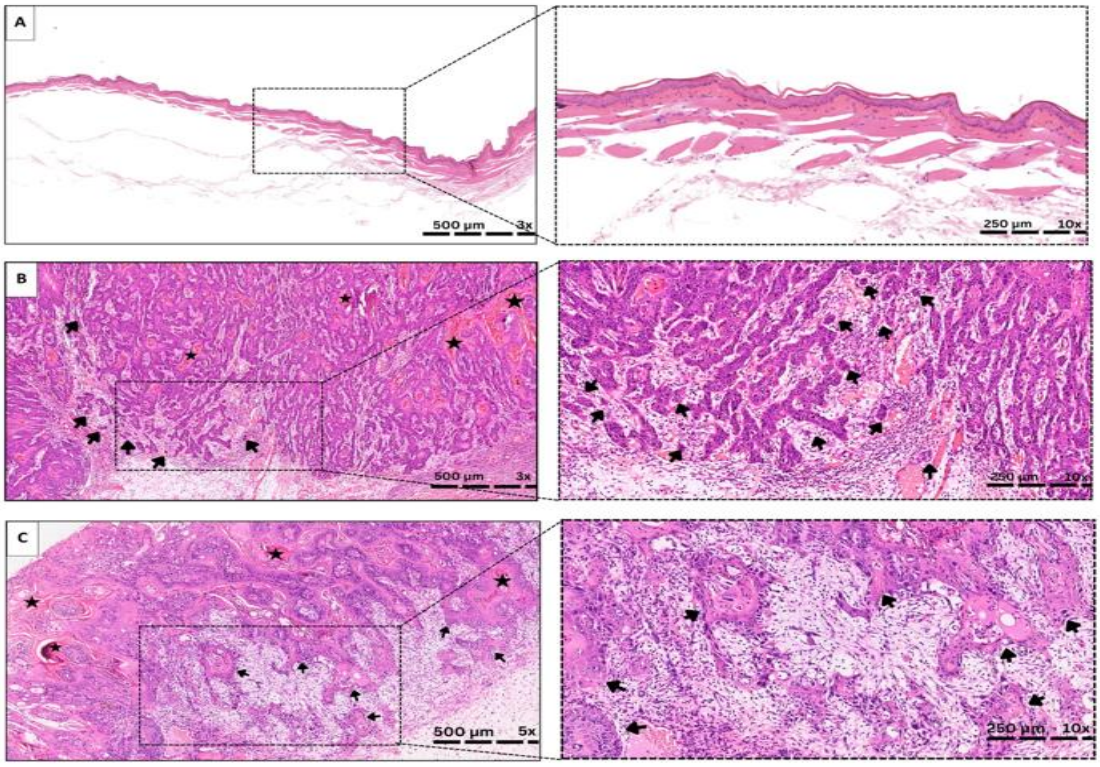

Figure 2: Histological analysis (H&E staining) of HBP tissue from negative control, positive control, and treated groups. (A) Group A (negative control) exhibits normal HBP architecture, consisting of 2–4 layers of keratinized stratified squamous epithelium overlying non-inflamed connective tissue and a mature striated muscle layer. (B) Group B (positive control) displays a deeply invasive, moderately differentiated exophytic tumor with aggressive tissue infiltration (black arrows) and

Tianjin Daxue Xuebao (Ziran Kexue yu Gongcheng Jishu Ban)/
Journal of Tianjin University Science and Technology
ISSN (Online):0493-2137
E-Publication: Online Open Access
Vol: 59 Issue: 08:2026
DOI: 10.5281/zenodo.22122654

prominent keratin pearl formation (black stars). (C) Group C (Cr-Pip-treated, 1 week) shows a moderately differentiated tumor with more cohesive tumor islands and a less invasive growth pattern at the tumor front (black arrows), along with keratin pearls (black stars), compared with Group B

3.4 Immunohistochemical analysis

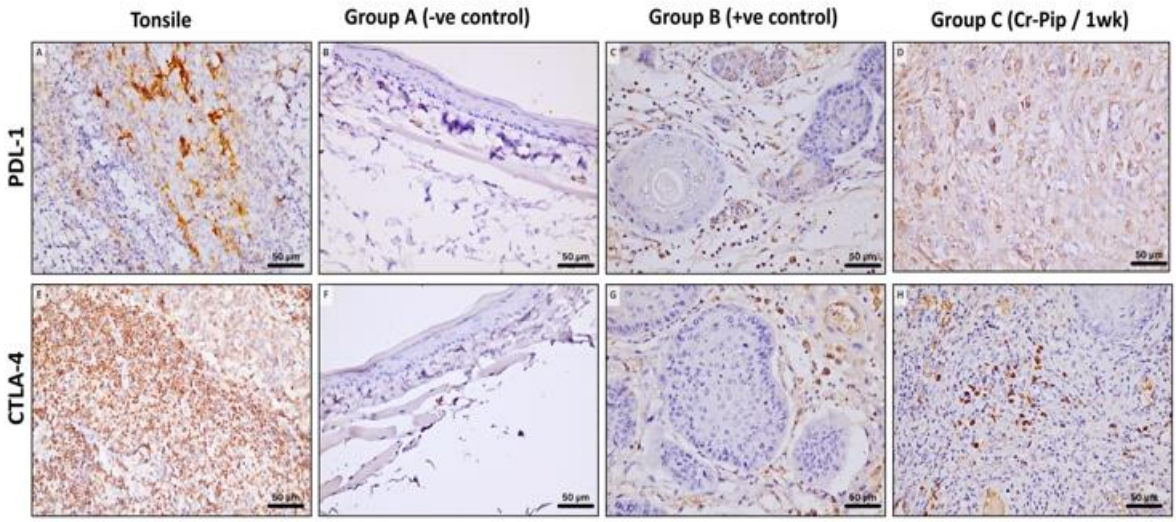

Figure 3: Representative photomicrographs of PDL-1 and CTLA-4 immunohistochemical staining across tonsil (positive tissue control) and experimental groups. (A) Tonsil tissue shows strong membranous and cytoplasmic PDL-1 immunoreactivity in lymphoid cells, confirming assay specificity. (B) Group A (negative control) shows absent PDL-1 expression within normal epithelium. (C) Group B (positive control) demonstrates focal PDL-1 immunoreactivity in tumor and stromal cells. (D) Group C (Cr-Pip-treated, 1 week) shows increased PDL-1 immunoreactivity with emergence of membranous expression in tumor cells. (E) Tonsil tissue exhibits diffuse, strong CTLA-4 immunoreactivity in lymphoid tissue, serving as a positive control. (F) Group A shows negligible CTLA-4 expression in normal tissue of HBP. (G) Group B demonstrates CTLA-4 immunoreactivity, restricted to scattered immune cells. (H) Group C shows a marked increase in CTLA-4-positive immune cell infiltration within the tumor stroma relative to Group B

To further characterize the immune checkpoint response to Cr-Pip treatment, PDL-1 and CTLA-4 expression was evaluated immunohistochemically, using tonsil tissue as a positive control tissue (**Fig. 3A&E**), with subsequent quantitative image analysis performed to compare expression levels between group B and group C **(Tab.1)** (**Fig.4**).

Group A (negative control) showed absence of PDL-1 expression within normal HBP epithelium (**Fig. 3B**). In group B (positive control), PDL-1 immunoreactivity was focally present within both tumor cells and the surrounding stromal cells (**Fig. 3C**). Following Cr-Pip treatment, group C demonstrated increased PDL-1 immunoreactivity, with the emergence of distinct membranous expression in tumor cells not prominently observed

Tianjin Daxue Xuebao (Ziran Kexue yu Gongcheng Jishu Ban)/
Journal of Tianjin University Science and Technology
ISSN (Online):0493-2137
E-Publication: Online Open Access
Vol: 59 Issue: 08:2026
DOI: 10.5281/zenodo.22122654

in Group B (**Fig. 3D**). Quantitative image analysis confirmed these qualitative observations (**Fig. 4A**). The TPS for PDL-1 was significantly higher in group C compared to group B ($p < 0.01$). Similarly, the ICS for PDL-1 was significantly elevated in group C relative to group B ($p < 0.01$).

Group A displayed negligible CTLA-4 expression within normal HBP tissue (**Fig. 3F**). Group B exhibited CTLA-4 immunoreactivity restricted to immune cells within the tumor microenvironment (**Fig. 3G**), whereas group C demonstrated a marked increase in CTLA-4-positive immune cell infiltration within the tumor stroma relative to group B (**Fig. 3H**). This qualitative increase was corroborated by quantitative analysis (**Fig. 4B**), which showed a significant elevation in CTLA-4 expression in group C compared with group B ($p < 0.05$).

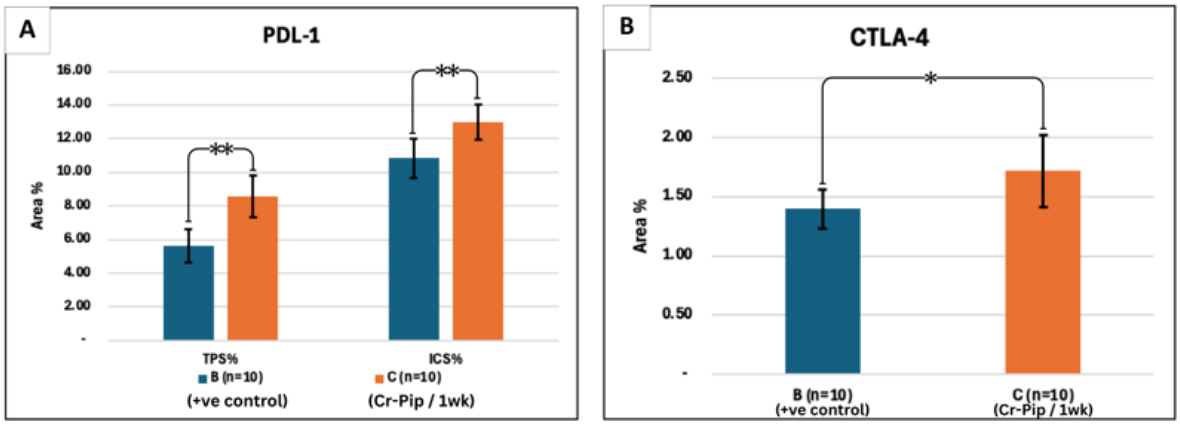

Figure 4: Quantitative image analysis of PDL-1 and CTLA-4 immunohistochemical expression in Group B (positive control) and Group C (Cr-Pip-treated, 1 week). (A) PDL-1 expression quantified as tumor proportion score (TPS%) and immune cell score (ICS%), expressed as mean area percentage ± SD. Both TPS% and ICS% were significantly higher in Group C compared with Group B. (B) CTLA-4 expression was quantified as mean area percentage ± SD, showing a significant increase in Group C relative to Group B. Statistical significance was determined by Mann-Whitney U test (*p < 0.05, **p < 0.01)

4. DISCUSSION

The present study evaluated the effects of a short-term, intraperitoneally administered Cr-Pip combination on tumor progression, systemic cytokine profile, histopathological architecture, and immune checkpoint expression in a DMBA-induced OSCC in the hamster model. Treatment was associated with reduced tumor burden and attenuated tumor-associated weight loss, a shift in serum cytokine profile characterized by reduced IL-10 alongside elevated TNF-α, a more cohesive and less invasive histological growth pattern, and a consistent increase in both PDL-1 and CTLA-4 expression within the tumor microenvironment.

Tianjin Daxue Xuebao (Ziran Kexue yu Gongcheng Jishu Ban)/
Journal of Tianjin University Science and Technology
ISSN (Online):0493-2137
E-Publication: Online Open Access
Vol: 59 Issue: 08:2026
DOI: 10.5281/zenodo.22122654

Tumor-bearing animals in group B exhibited significant weight loss relative to the negative control group, consistent with the systemic catabolic effects commonly observed in carcinogen-induced tumor models, which are frequently attributed to tumor-associated cachexia driven by chronic inflammatory cytokine release and increased metabolic demand [19]. The reduction in tumor size aligns with previous reports describing antiproliferative and growth-inhibitory effects of Cr in chemically induced oral carcinogenesis models, generally attributed to suppression of NF-κB-dependent proliferative signaling and induction of apoptotic pathways in tumor cells through cytochrome c release, and activation of caspase-3 [20][21]. The addition of Pip, which enhances Cr bioavailability through inhibition of hepatic glucuronidation, may have contributed to achieving a measurable biological effect within the comparatively one-week treatment period used in the present study [22].

The observed significant reduction in serum IL-10 following treatment is consistent with a shift away from the immunosuppressive cytokine milieu typically associated with tumor progression, since IL-10 is well recognized for its role in dampening cytotoxic T-cell responses and promoting tumor immune evasion [23]. TNF-α is a pleiotropic cytokine in cancer biology; it can be produced by activated macrophages and T cells as part of an effective anti-tumor inflammatory response, but it can equally contribute to tumor-promoting chronic inflammation depending on the surrounding cytokine network and duration of exposure [24]. In the context of the present findings, the coexistence of reduced tumor bulk, decreased IL-10, and increased TNF-α is more consistent with a shift toward a locally activated, pro-inflammatory immune response than with a purely destructive inflammatory process.

The histological findings provide additional support for a treatment-associated shift in tumor behavior rather than complete tumor regression. Group C tumors retained moderate differentiation and keratin pearl formation, indicating that Cr-Pip treatment did not eliminate the neoplastic phenotype within one week, but the tumor islands were more cohesive and the invasive front displayed a less aggressive growth pattern than in untreated tumor-bearing animals [25]. The relatively preserved cohesion observed in the treated group is therefore biologically consistent with a reduced invasive phenotype, and aligns conceptually with previous reports describing curcumin's capacity to downregulate matrix metalloproteinase activity and epithelial-mesenchymal transition-associated signaling in oral cancer cell models [26].

The most striking finding of this study is the significant increase in both PDL-1 and CTLA-4 expression in Cr-Pip-treated animals compared with untreated tumor-bearing controls. This finding is consistent with the well-established phenomenon of adaptive immune resistance, in which PDL-1 expression on tumor and stromal cells is upregulated in direct response to local immune cell activation, most notably through interferon-γ secreted by infiltrating cytotoxic T lymphocytes [27]. This interpretation is consistent with the concurrent reduction in tumor size and the more cohesive, less invasive histological pattern observed in the same treated animals. It is also consistent with the reduction in IL-10, an immunosuppressive cytokine, alongside the increase in TNF-α, since both

Tianjin Daxue Xuebao (Ziran Kexue yu Gongcheng Jishu Ban)/
Journal of Tianjin University Science and Technology
ISSN (Online):0493-2137
E-Publication: Online Open Access
Vol: 59 Issue: 08:2026
DOI: 10.5281/zenodo.22122654

changes are compatible with a more immunologically active tumor microenvironment [28]. The present findings about increased PDL-1 and CTLA-4 expression by Cr-Pip treatment raise the possibility that such treatment could sensitize OSCC to subsequent or combined immune checkpoint inhibitor therapy, since tumors with low baseline checkpoint expression are generally less responsive to checkpoint blockade than those with an actively engaged, checkpoint-expressing immune microenvironment [29].

Future studies should extend the treatment duration to evaluate whether the histological and immunological changes observed here are sustained, amplified, or reversed over longer exposure periods. Direct immunophenotyping of tumor-infiltrating lymphocyte populations, as well as assessment of interferon-γ and other T-cell effector cytokines within tumor tissue, would help to directly test the adaptive immune resistance hypothesis proposed here. Finally, combination studies evaluating Cr-Pip treatment alongside immune checkpoint inhibitor therapy would represent a promising avenue for future investigation.

5. CONCLUSION

In summary, short-term Cr-Pip treatment reduced tumor burden and produced histological evidence of a less invasive tumor phenotype in a DMBA-induced hamster model of OSCC, changes accompanied by a shift in serum cytokine balance and increased PDL-1 and CTLA-4 expression within the tumor microenvironment. These checkpoint changes are more consistent with a treatment-associated increase in local immune engagement. These findings support continued investigation of Cr-Pip as a modulator of both tumor behavior and the tumor immune checkpoint in oral carcinogenesis.

Declaration of interests

The authors declare no known competing financial interests or personal relationships that could have influenced the work presented in this paper.

References

1) Tan Y, Wang Z, Xu M, Li B, Huang Z, Qin S, et al. Oral squamous cell carcinomas: state of the field and emerging directions. Int J Oral Sci 2023;15:44–67. https://doi.org/https://doi.org/10.1038/s41368-023-00249-w.

2) Alonso-Juarranz M, Mascaraque M, Carrasco E, Gracia-Cazaña T, De La Sen O, Gilaberte Y, et al. The distinctive features behind the aggressiveness of oral and cutaneous squamous cell carcinomas. Cancers (Basel) 2023;15:3227–44. https://doi.org/10.3390/cancers15123227.

3) Caruntu A, Yang SF, Acero J. New insights for an advanced understanding of the molecular mechanisms in oral squamous cell carcinoma. Int J Mol Sci 2024;25:6964. https://doi.org/https://doi.org/10.3390/ijms25136964.

4) Monti-Hughes A, Aromando RF, Pérez MA, Schwint AE, Itoiz ME. The hamster cheek pouch model for field cancerization studies. Periodontol 2000 2015;67:292–311. https://doi.org/10.1111/prd.12066.

5) Andersen ML, Winter LMF. The hamster model of sequential oral carcinogenesis: an update. An Acad Bras Cienc 2019;33:1751–5. https://doi.org/10.1590/0001-3765201720170238.

Tianjin Daxue Xuebao (Ziran Kexue yu Gongcheng Jishu Ban)/
Journal of Tianjin University Science and Technology
ISSN (Online):0493-2137
E-Publication: Online Open Access
Vol: 59 Issue: 08:2026
DOI: 10.5281/zenodo.22122654

6) Pellicioli ACA, Bingle L, Farthing P, Lopes MA, Martins MD, Vargas PA. Immunosurveillance profile of oral squamous cell carcinoma and oral epithelial dysplasia through dendritic and T-cell analysis. Journal of Oral Pathology and Medicine 2017;46:928–33. https://doi.org/10.1111/jop.12597.

7) Kostecki KL, Iida M, Crossman BE, Salgia R, Harari PM, Bruce JY, et al. Immune escape strategies in head and neck cancer: evade, resist, inhibit, recruit. Cancers (Basel) 2024;16:312–42. https://doi.org/10.3390/cancers16020312.

8) Qin W, Hu L, Zhang X, Jiang S, Li J, Zhang Z, et al. The diverse function of PD-1/PD-L pathway beyond cancer. Front Immunol 2019;10:2298–314. https://doi.org/10.3389/fimmu.2019.02298.

9) Yan Q, Zhang B, Ling X, Zhu B, Mei S, Yang H, et al. CTLA-4 facilitates DNA damage–induced apoptosis by interacting with PP2A. Front Cell Dev Biol 2022;10:728771–86. https://doi.org/10.3389/fcell.2022.728771.

10) Lemma EY, Letian A, Altorki NK, McGraw TE. Regulation of PD-L1 trafficking from synthesis to degradation. Cancer Immunol Res 2023;11:866–74. https://doi.org/10.1158/2326-6066.CIR-22-0953.

11) Deng LJ, Qi M, Li N, Lei YH, Zhang DM, Chen JX. Natural products and their derivatives: Promising modulators of tumor immunotherapy. J Leukoc Biol 2020;108:493–508. https://doi.org/10.1002/JLB.3MR0320-444R.

12) Yoysungnoen-Chintana P, Bhattarakosol P, Patumraj S. Antitumor and antiangiogenic activities of curcumin in cervical cancer xenografts in nude mice. Biomed Res Int 2014;2014:817972–84. https://doi.org/10.1155/2014/817972.

13) Lee SY, Cho SS, Li YC, Bae CS, Park KM, Park DH. Anti-inflammatory effect of curcuma longa and allium hookeri co-treatment via NF-κB and COX-2 pathways. Sci Rep 2020;10:5718–29.

14) Zhu L, Han MB, Gao Y, Wang H, Dai L, Wen Y, et al. Curcumin triggers apoptosis via upregulation of Bax/Bcl-2 ratio and caspase activation in SW872 human adipocytes. Mol Med Rep 2015;12:1151–6. https://doi.org/10.3892/mmr.2015.3450.

15) Lopresti AL. The problem of curcumin and its bioavailability: could its gastrointestinal influence contribute to its overall health-enhancing effects? Advances in Nutrition 2018;9:41–50. https://doi:10.1093/advances/nmx011.

16) Arcaro CA, Gutierres VO, Assis RP, Moreira TF, Costa PI, Baviera AM, et al. Piperine, a natural bioenhancer, nullifies the antidiabetic and antioxidant activities of curcumin in streptozotocin-diabetic rats. PLoS One 2014;9. https://doi.org/10.1371/journal.pone.0113993.

17) Ulas EB, Hashemi SMS, Houda I, Kaynak A, Veltman JD, Fransen MF, et al. Predictive value of combined positive score and tumor proportion score for immunotherapy response in advanced NSCLC. JTO Clin Res Rep 2023;4:100532. https://doi.org/10.1016/j.jtocrr.2023.100532.

18) Anand N, Srivastava P, Husain N, Agarwal D, Gupta A, Pradhan R. Evaluation of CTLA-4 and PD-L1 expression in thyroid carcinoma and its prognostic significance. Cureus 2024;16. https://doi.org/10.7759/cureus.67004.

19) Baracos VE, Martin L, Korc M, Guttridge DC, Fearon KCH. Cancer-associated cachexia. Nat Rev Dis Primers 2018;4:1–18. https://doi.org/10.1038/nrdp.2017.105.

20) Lin YG, Kunnumakkara AB, Nair A, Merritt WM, Han LY, Armaiz-Pena GN, et al. Curcumin inhibits tumor growth and angiogenesis in ovarian carcinoma by targeting the nuclear factor-κB pathway. Clinical Cancer Research 2007;13:3423–30. https://doi.org/10.1158/1078-0432.CCR-06-3072.

21) Hu A, Huang JJ, Zhang JF, Dai WJ, Li RL, Lu ZY, et al. Curcumin induces G2/M cell cycle arrest and apoptosis of head and neck squamous cell carcinoma in vitro and in vivo through ATM/Chk2/p53-dependent pathway. Oncotarget 2017;8:50747–60. https://doi.org/10.18632/oncotarget.17096.

Tianjin Daxue Xuebao (Ziran Kexue yu Gongcheng Jishu Ban)/
Journal of Tianjin University Science and Technology
ISSN (Online):0493-2137
E-Publication: Online Open Access
Vol: 59 Issue: 08:2026
DOI: 10.5281/zenodo.22122654

22) Kumar S, Singhal V, Roshan R, Sharma A, Rembhotkar GW, Ghosh B. Piperine inhibits TNF-α induced adhesion of neutrophils to endothelial monolayer through suppression of NF-κB and IκB kinase activation. Eur J Pharmacol 2007;575:177–86. https://doi.org/10.1016/j.ejphar.2007.07.056.

23) Rivas JR, Liu Y, Alhakeem SS, Eckenrode JM, Marti F, Collard JP, et al. Interleukin-10 suppression enhances T-cell antitumor immunity and responses to checkpoint blockade in chronic lymphocytic leukemia. Leukemia 2021;35:3188–200. https://doi.org/10.1038/s41375-021-01217-1.

24) Cruceriu D, Baldasici O, Balacescu O, Berindan-Neagoe I. The dual role of tumor necrosis factor-alpha (TNF-α) in breast cancer: molecular insights and therapeutic approaches. Cellular Oncology 2020;43:1–18. https://doi.org/10.1007/s13402-019-00489-1.

25) Mishra A, Das A, Dhal I, Shankar R, Bhavya BM, Singh N, et al. Worst pattern of invasion in oral squamous cell carcinoma is an independent prognostic factor. J Oral Biol Craniofac Res 2022;12:771–6. https://doi.org/10.1016/j.jobcr.2022.08.027.

26) Lee AYL, Fan CC, Chen YA, Cheng CW, Sung YJ, Hsu CP, et al. Curcumin inhibits invasiveness and epithelial-mesenchymal transition in oral squamous cell carcinoma through reducing matrix metalloproteinase 2, 9 and modulating p53-E-cadherin pathway. Integr Cancer Ther 2015;14:484–90. https://doi:10.1177/1534735415588930.

27) Berry S, Taube JM. Innate vs. adaptive: PD-L1-mediated immune resistance by melanoma. Oncoimmunology 2015;4:e1029704–7. https://doi.org/10.1080/2162402X.2015.1029704.

28) Gómez-Valenzuela F, Escobar E, Pérez-Tomás R, Montecinos VP. The inflammatory profile of the tumor microenvironment, orchestrated by cyclooxygenase-2, promotes epithelial-mesenchymal transition. Front Oncol 2021;11:686792. https://doi.org/10.3389/fonc.2021.686792.

29) Fan P, Qi Z, Liu Z, Wang S, Wang Y, Kuai J, et al. High baseline levels of PD-L1 reduce the heterogeneity of immune checkpoint signature and sensitize anti-PD1 therapy in lung and colorectal cancers. Cell Death Dis 2025;16:152. https://doi.org/10.1038/s41419-025-07471-w.